Forces in Mechanics 13 (2023) 100232

Contents lists available at ScienceDirect

Forces in Mechanics

journal homepage: www.sciencedirect.com/journal/forces-in-mechanics

Exploring the capability of acoustic emission technique in early detecting mode I and mixed mode fractures

Giulia Boccacci [a], Francesca Frasca [a], Pasi Aalto [b], Chiara Bertolin [c,*], Anna Maria Siani [a]

[a] Department of Earth Sciences, Sapienza University of Rome, P.le Aldo Moro, 5, 00185, Rome, Italy
[b] Department of Architecture and Technology, Norwegian University of Science and Technology, Sentralbygg 1, NTNU Wood (220, 2.etg), 7491 Trondheim, Norway
[c] Department of Mechanical and Industrial Engineering, Norwegian University of Science and Technology, Richard Birkelands vei 2B, 7491 Trondheim, Norway

ARTICLE INFO

Keywords:
Acoustic Emission
Digital Image Correlation
Universal Testing Machine
Non-destructive techniques
Grain angle
Tree rings number
Wood
Softwood
Scots pine
Early warning

ABSTRACT

Acoustic Emission non-destructive technique was used coupled with Digital Image Correlation to explore its early warning capability in detecting Mode I and mixed Mode fractures in Scots pine samples. The acoustic behaviour of the specimens, being different for tree rings number (high and low) and grain angle (0-20-40-60°), was investigated while undergoing an external tensile load by a Universal Testing Machine. A risk amplitude threshold (51.9 dB) was experimentally computed *a posteriori* as an early warning indicator for Scots pine samples with mixed Mode fractures. In the case of Mode I fracture, as cracks occur instantaneously, the oncoming fracture could not be predicted.

1. Introduction

New and sophisticated techniques in the field of preventive conservation of cultural heritage provide the opportunity to monitor materials that are vulnerable, and to develop early warning methods which may help to know in advance when degradation of the material begins or to localise structural fragility. The application of such techniques aims to increase the knowledge on the actual conservation state of heritage objects such as paintings, textiles, manuscripts, wooden artifacts, etc. These techniques are fundamental to support conservation activities but also for understanding how the degradation processes are triggered by surrounding environmental conditions. In the case of structural health monitoring of objects made of wood, the most widely used non-destructive testing (NDT) techniques for the assessment of timber structures are visual, acoustic, vibration, strength or moisture grading probing techniques [1].

Wood fracture depends on the modes of loading and on the direction of crack propagation, due to the anisotropy of wooden structures and properties. The three pure modes of fracture are: Mode I - opening or tensile mode, in which the crack surfaces move directly apart (i.e., stress is orthogonal to the local plane of the crack surface); Mode II - sliding or in-plane shear mode, in which the crack surfaces slide across one another in the direction perpendicular to the leading edge of the crack (i.e., stress parallel to the crack surface but orthogonal to the crack front); Mode-III tearing or anti-plane shear mode, in which the crack surfaces move parallel to the leading edge of the crack (i.e., stress parallel to the crack surface and to the crack front); while the mixed Mode fracture involves a combination of two to three of the pure modes [2].

Since the direction parallel to the wood grain offers the least resistance to crack propagation, fractures tend to grow in this direction. The loading mode applied to a wooden sample causes a fracture defined Mode I, if the grain angle (defined as the angle between the wood fibre direction and the vector in axial direction) is 0°, which means grain parallel to the axial direction. As the grain angle increases, the fracture can be described by a mixed Mode, until it turns into Mode II when it reaches 90°. Moreover, it is worth mentioning that the fracture toughness perpendicular to the grain is approximately one order of magnitude greater than that parallel to the grain [3]. In field of wooden fracture under mixed Mode I/II many studies have been done employing analytical, numerical, and experimental approaches. A comprehensive fracture characterisation of wood components via experimental and numerical approaches has been proposed by Moura et al.; they proposed equivalent crack concept to obtain cohesive crack properties in Mode I with different standard test specimens (i.e., three-point bending

* Corresponding author.
E-mail address: chiara.bertolin@ntnu.no (C. Bertolin).

https://doi.org/10.1016/j.finmec.2023.100232
Received 15 May 2023; Received in revised form 1 August 2023; Accepted 18 August 2023
Available online 27 August 2023

(SEN-TPB) [4], double cantilever beam (DCB) [5] and tapered double cantilever beam (TDCB) [6]). In their studies, the crack length and elastic properties were calculated by a data reduction method. Another method was also proposed by Yoshihara [7] by using the four-point bend end-notched flexure (4-ENF) specimens of Spruce to extract Mode II fracture toughness as a function of crack length or Mode II R-curve with a data reduction method. In another study, Yoshihara demonstrated that the previously proposed method [7] was able to obtain the relation between the Mode II energy release rate and crack length [8]. Stanzl-Tschegg's group studied Mode I fracture of different wood species in different crack propagation systems and showed a significant influence of geometrical factors of a specimen and crack orientation on the values of fracture toughness determined experimentally [9,10]. Fakoor and Mehri investigated the fracture of composite materials and proposed a new method to estimate the Mode II fracture toughness. They discussed the effect of the fracture process zone (FPZ) on the Mode II fracture toughness [11]. Fracture mechanics approaches are gaining more prominence, namely the methods based on appropriate fracture criteria and simulation of the failure behaviour by associated models, however, an overview of the mixed Mode I/II criteria for fracture investigation of composite materials was already provided by [12].

Among the several portable NDT techniques which, during structural health monitoring of timber structures, are capable to discriminate the fracture modes, Acoustic Emission (AE) seems the most promising technique. It is currently used to study the mechanism of damage occurring at certain stress levels in wood, as extensively reported by Baensch [13]. The AE applied to monitor wooden samples, is mainly used in laboratory experiments, as highlighted in Boccacci *et al.* [1], while a very limited number of studies are dealing with the monitor of movable wooden objects *in situ*, specifically wooden furniture [14]. During tests, the AE instrumentation is often found coupled with the Universal Testing Machine, mainly to perform fracture tests, but also tensile, cutting, compressive and torsional tests on the samples, and with the Digital Image Correlation often used to record images during the experiments. In laboratory tests, wood samples can be subjected to pre- or ongoing experimental settings procedures, such as acclimatisation at given temperature and relative humidity in climate chamber [15–17], or in dryer chamber [18], or simply moistening in water [19–21]. The multi-techniques approach frequently used in this field appears to be lacking in microscopic observations, although they have proved to be very effective in fractography, i.e., a method for studying the fracture of materials in failure analysis (as in the case of the use of scanning electron microscopy systems with wood [22–25]). Additionally, theoretical approaches are often explored in parallel with the experimental ones, with the aim of obtaining modelling and generalisation e.g., through numerical simulation by using Finite Element Analysis [16,26–28] or mathematical formulations [23,29–31]. The AE technique can be also employed to perform damage characterization in composite materials. Many authors in fact, established the links between composite material's failure features and the AE signals, determining each failure mode of the composites under different loading processes. However, AE signals generated by heterogeneous materials are not stationary. Moreover, combining the merits of different methodologies (i.e., Digital Image Correlation, Ultraviolet Visible spectroscopy etc.) to that of Acoustic Emission in a multi-technique analysis it was proven to dramatically improve the reliability of AE investigation [32–34].

Looking in detail at the AE activity recorded in softwood samples as one of the widely used building construction materials in Scandinavian Countries [1], it emerged that although not thoroughly investigated, high/low tree ring density and grain angle can be influencing factors to be analysed in depth [20,23,6,10].

When the tree ring density has a homogeneous anatomical structure, AE signals are numerous and of low energy. In contrast, AE signals can be very emissive and/or energetic [15]. In addition, it was found that in spruce samples latewood emitted much more AE signals than spruce earlywood (because of a higher tracheid number) [19]. Moreover, AE signals are highly affected by the grain angle of different wood species [20]: e.g., AE counts decrease from 0° to 45° and increase from 45° to 90° [35].

The present research aims to evaluate the capability of AE NDT technique in the early detection of modes of fracture occurring in wooden samples, when subjected to the application of an external load. The AE activity of Scots pine samples is here investigated in relation to the crack length measurements recorded by a Digital Image Correlation camera during tensile tests. Particular attention is paid to the tree rings number (TRN) and to the grain angle (GA), features that are considered as influencing factors in the acoustic activity recorded and therefore on its early warning potential [1].

The paper is structured in three sections: "Materials and Methods" reports the detailed description of tested materials and the equipment used in the experiments, as well as the steps followed to elaborate data, and to design the novel early warning method proposed. In "Results and Discussion", the outcomes of the preliminary analysis are provided, and the results related to the early warning method developed here are discussed. Then, "Conclusions" reports the findings and discusses the implications of the achieved results.

2. Materials and methods

2.1. Scots pine wood samples

The tested material was a set of specimens obtained from two large boards of Scots pine, a wooden species characterised by a density ranging between 505 kg/m^3 and 540 kg/m^3, and the moisture content range between 12.0% and 12.4% [36]. The two boards were industrially dried and each of them had a different number of tree rings along the length of the sample. The samples were divided into groups (low and high) based on the tree rings number (TRN) visually counted within the linear length of each sample (100 mm). The former includes samples with TRN equal or lower than 11, the latter includes samples with TRN higher than 11.

The set of samples included 15 pieces free of defects that were cut as SENT (single edge notch tension) specimens at the Wood Centre of the Norwegian University of Science and Technology (NTNU, Trondheim, Norway) in April 2021. The one-sided initial notch of 14 mm length and 0.3 mm width was applied at mid-length of each specimen by means of a new fine carpentry pull saw (i.e., factory sharpened) so that each specimen would start with the same initial crack geometry. The cut was applied using an angle jig and stopper to ensure consistency of the cuts across samples. Each sample was control measured using a caliper. The samples used for the present work were cut from the boards in the radial longitudinal (RL) direction (as shown in Fig. 1a), which corresponds to the cut along the longitudinal axis. Their dimensions were 100 mm x 35 mm x 10 mm (length × width × height, as shown in Fig. 1b).

The notch was oriented in the parallel direction with respect to the grain angle, as shown in Fig. 2, where the samples were further subdivided into four categories according to their grain angle (GA) values (i.e., 0°, 20°, 40° and 60°). The zero-degree angle was specifically chosen as representative of Mode I fracture, while the other angles were chosen to study how the mechanical characteristics varied, as well as the detectability by AE technique in accordance with an increasing mixed Mode of fracture.

The specimens were named with the letter "H" or "L" indicating high or low TRN, respectively, followed by the GA number (0°, 20°,40° and 60°) and by the letters "PA" indicating the parallel direction of the notch with respect to the grain. The last character was the number of specimens obtained for each group. A few samples were not considered in the further analysis of the raw data due to their microscopic structure and/or the anomalies occurred during the data detection in the laboratory experiments. Table 1 shows the specimens tested for each TRN group and for each GA category.

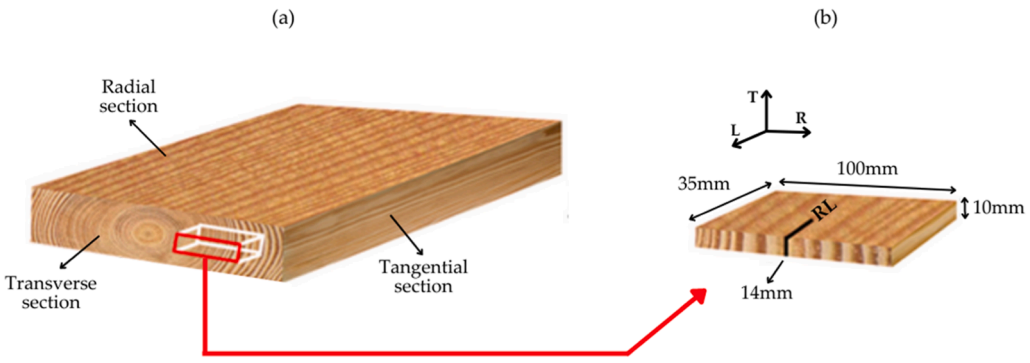

Fig. 1. (**a**) Illustration of the Scots pine wood board with fundamental sections; (**b**) Illustration of the SENT sample with the anatomic directions (T=tangential, L=longitudinal and R=radial) and dimensions.

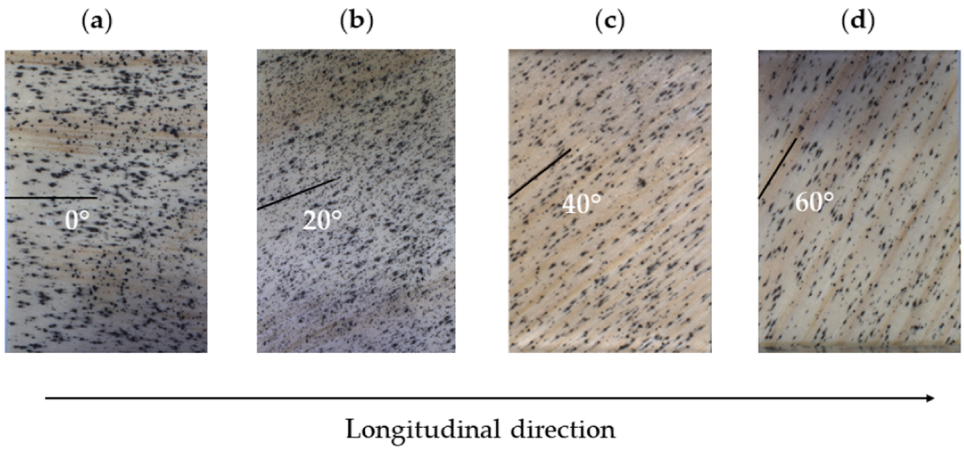

Fig. 2. Samples with pre-crack notch parallel to (**a**) 0° grain angle, (**b**) 20° grain angle, (**c**) 40° grain angle and (**d**) 60° grain angle with respect to the axial direction. Sample size:100 mm x 35 mm x 10 mm.

Table 1
Designation of the samples included in the analysis and corresponding tree rings number (TRN) group and grain angle (GA) category.

Samples	Tree Rings Number		Grain angle (°)
H00PA5	HIGH	12	0
H20PA4		13	20
H40PA4		18	40
H40PA6		18	
H40PA7		22	
H60PA5		24	60
H60PA6		23	
L00PA5	LOW	4	0
L20PA4		4	20
L40PA4		9	40
L40PA5		8	
L40PA6		8	
L60PA4		10	60
L60PA5		4	
L60PA6		9	

2.2. Equipment

Fig. 3 schematically shows the equipment (Universal Testing Machine, DIC camera and AE detector) employed to test Scots pine samples, their set-up, and the list of parameters used for the following analysis.

The Universal Testing Machine (UTM of 5kN by MTS producer) was used to perform tensile tests on the samples with a displacement rate of 0.5 mm/min [37]; experiments took place at the Norwegian University of Science and Technology (NTNU, Trondheim, Norway), in April-May 2021.

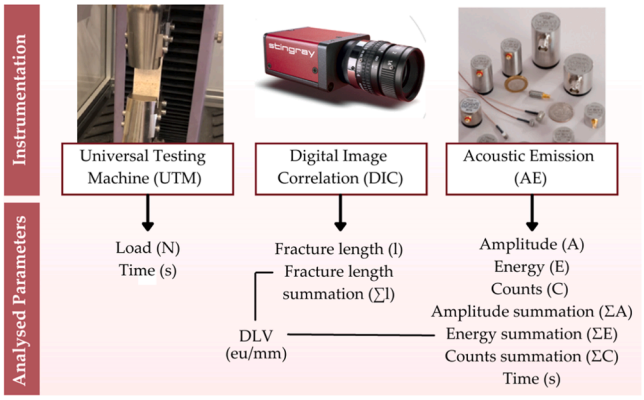

Fig. 3. Scientific instruments used in the experiments and analysed parameters.

The fracture initiation and propagation occurring during the experimental tests were evaluated over time by means of a commercial Digital Image Correlation (DIC) system VIC-2D 7 (Correlated Solutions Inc.) together with its high-resolution camera (Stringray_F-504) [38] taking about 20 frames/s. Before starting the experiments, a random pattern of roughly circular "speckles" of uniform size and random locations was created on the specimens (Fig. 2). The high contrast produced by means of an airbrush filled with black ink over the base material was helpful in creating reference points to detect the fracture propagation and the related fracture process zone (FPZ). The set-up of VIC-2D 7 system followed the company's instruction to prepare our tests and generate

high-quality data for post-process. The collected images were analysed through Surfer ® 9.0 (distributed by Golden Software) to measure the length of the fractures.

The AMSY-6 (manufactured by Vallen System) allowed us to detect the Acoustic Emission activity emitted by the samples under stress, by means of one single sensor positioned in the back side of each sample. Amplitude (A), Counts (C) and Energy (E) were recorded and investigated in this study as the most important AE parameters in the time domain [39].

2.3. Data pre-processing and analysis

The outputs obtained by the three instruments AE, UTM and DIC for each sample were synchronised in time and AE raw data were filtered by all the signals below 40 dB to discriminate only real AE events from spurious noise signal. Samples showing missing data or particularly high environmental or electronic background noise were excluded from the analysis. Indeed, these data were not representative of a real acoustic activity caused by the application of external load.

After that, in accordance with the procedure described in [40], the completeness index (*CoI*) was calculated to assess the completeness of the raw data analysed. *CoI* was determined by using Eq. (1), as the ratio between the number of good measurements (*Nr*) (i.e., not affected by poor instrumental performance) and the total numbers of the series (*TN*). The *CoI* ranges from 1 (excellent instrumental performance) to 0 (very poor instrumental performance).

$$CoI = \frac{Nr}{TN} \tag{1}$$

The length of the propagating fractures was measured in pixels, taking the width value of the samples as reference (35 mm), and the pixels were converted into millimetres, using the proportion 1 pixel ~ 0.04 mm (±1 mm for GA=0-20° and ±2 mm for GA=40-60°). The length of the fracture (l) as a function of time (t) was derived frames by frames for each sample (Fig. 2). Sample images recorded through DIC were processed to enhance contrast between speckle pattern and raw sample background. This procedure was applied to all frames in order to identify the fracture process zone (FPZ).

The cumulative summations of fracture length (Σl), and AE parameters (Amplitude, Counts and Energy) were used to evaluate the individual trend of AE activity over time.

In addition, the load (L) applied to the tested materials, and the Density Linear energy Value (*DLV*), were used to study the energy release as the ratio between the cumulative sum of the energy released and the linear fracture (ΣE_{AE}) (Eq. 2, expressed in e.u./mm)[26].

$$DLV = \frac{\Sigma E_{AE}}{\Sigma l} \tag{2}$$

A single database for each sample, including all the variables obtained by the three instruments, was used to perform the following analysis.

2.4. Identification of the early warning (EW) detection method

At first, during the test, two main stages of the fracture process were discriminated for all the Scots pine samples. Consequently, each dataset was split into two time intervals:

- Δt_1: time elapsed between the start of the experiment and the crack initiation at macro-level.
- Δt_2: time elapsed between crack initiation and the instant of the complete fracture.

In order to detect an early warning (EW) stage in the acoustic activity recorded before the fracture process, the procedure was mainly focused on the analysis of data collected over the Δt_1 time interval.

At first, the evolution of fracture process was studied by computing the second derivative of the cumulative signals of AE parameters with respect to time for each sample. Then, a filter of 90th percentile was applied to discriminate abrupt changes in AE events before the crack initiation.

In addition, the persistence of intense AE signals was studied by computing the number of occurrences higher than the 68th percentile for each sample due to their deformation under the external load. The 68th percentile was chosen as the percentile within which the natural fluctuation of the measured variable lies (68% of the measures lies within 1 standard deviation of the mean in the normal distribution). We hypothesize that this filter allows to discriminate an EW acoustic activity before the crack initiation.

However, in a practical application it is not possible to calculate the 68th percentile in real-time during the monitoring of AE activity, because as soon as data begin to be stored, they progressively increase in number, changing the distribution as well as the 68th percentile value. Therefore, a threshold was then identified as the median value among the 68th percentiles of amplitude (A) computed for all the acoustic signals available from the samples. This threshold was experimentally calculated *a posteriori* as a general reference for all the Scots pine SENT samples considered in the present work. Particularly, this early warning threshold was used to predict at which time after it is exceeded, a crack occurs in the above-mentioned samples depending on different TRN and GAs (and so to their different modes of fracture). Therefore, the early warning time interval (Δt_{ew}) expressed in s, was found through Eq. (3), where t_{start} is the time at the crack initiation point and t_{ew} represents the time value at which the pre-crack acoustic activity exceeds the *a posteriori* set threshold (i.e., median value of 68th percentiles of the amplitude of all the samples).

$$\Delta t_{ew} = t_{start} - t_{ew} \tag{3}$$

3. Results and discussion

3.1. Data preprocessing and analysis

The completeness index (*CoI*) of the set of samples was high (*CoI*= 0.88), since 2 out of 17 tested samples were excluded from the analysis due to an intense AE activity derived from environmental and electronic noise.

Fig. 4 shows the speckle images of sample "H00PA5" (taken as an example) at three loading points: a) before crack initiation (black), b) after crack initiation (light blue), and c) at the end of the fracture process (red). The comparison puts in light the propagation of the fracture under load. However, a random speckle pattern applied on a light wooden sample through airbrush painting has not made it possible a clear discrimination of microcracks related to the development of a fracture process zone (FPZ). As the FPZ size does not affect AE signals before macro-crack initiation, it does not represent a limitation in exploring the capability of AE technique in early detecting Mode I and mixed Mode fractures.

Time plots of AE parameters (pure signal) and the corresponding cumulative curves allowed us to visualise the trend and to detect crack occurrence. In Fig. 5, the example of "H20PA4" sample (high tree rings number – 20° grain angle) is reported.

Points scattered at low amplitude (around 40 dB) showed in the time plot of pure signal amplitude parameter, could be due to mixed events (real events of low intensity and noise), while high amplitude values indicate real events occurred at the initiation of the crack and during its progression (similarly for the counts and for the energy parameters). In the cumulative curves in Fig. 5, the simultaneous vertical rise of the y-axis values provides the "temporal window" (x-axis) over which the crack propagation is expected to occur. When an increase of the cumulative values is not observed, it can be associated with absence of AE activity. All samples showed a similar pattern, with different values of

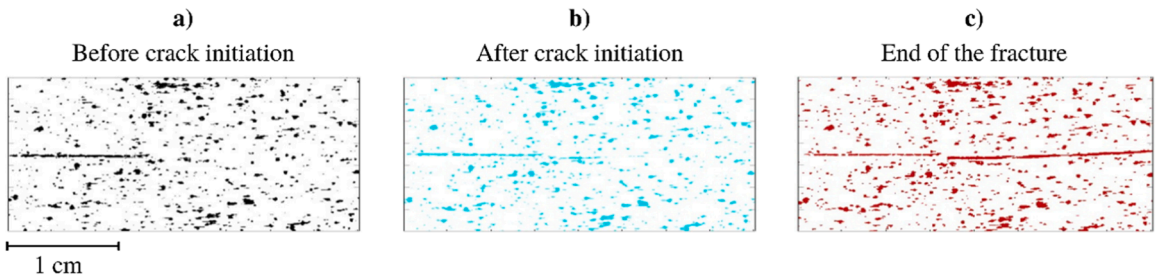

Fig. 4. Speckle pattern of sample "H00PA5" at three loading points. Subset size = 14 mm x 32 mm.

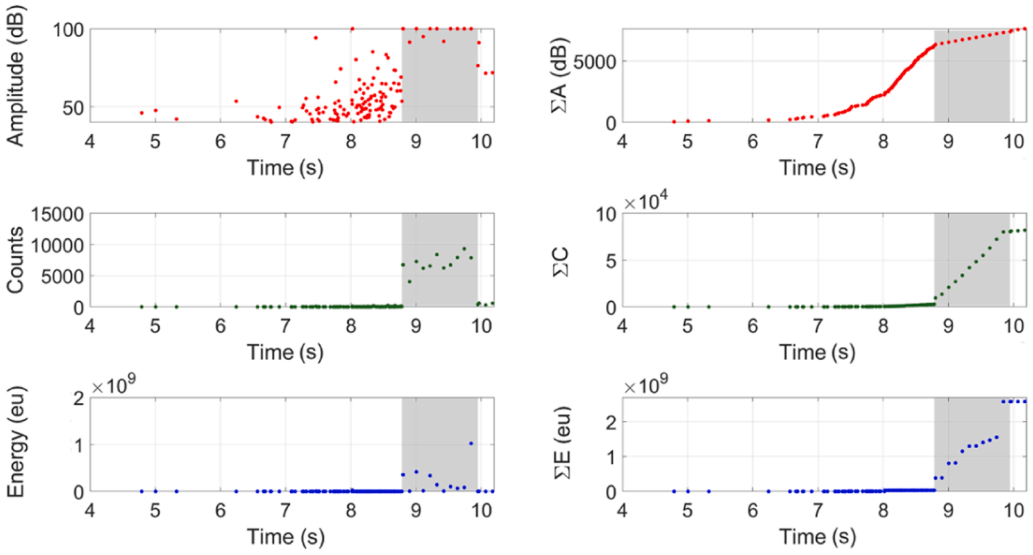

Fig. 5. Time plots of (left panels) AE parameters pure signals and (right panels) corresponding cumulative curves of the sample H20PA4. The grey areas highlight the temporal window over which the cracks propagation occur.

AE parameters and different extensions of time windows. Additionally, the amplitude parameter (A) – that reached saturation at 100 dB, during the occurrence of the fracture – has been seen to more clearly display the acoustic activity happening in every sample in advance with respect to the physical appearance of failure. For its greater sensitivity when compared to the other two AE output parameters (e.g., Counts and Energy), the Amplitude has been here considered as more useful in order to explore the capability of Acoustic Emission technique in early detecting Mode I and Mixed Mode fractures. Other authors reported the investigation on the Acoustic Emission Amplitude pa-rameter for the same purpose of evaluating pre-failure stages in different materials [41–44].

Concerning the frequency distribution (i.e., the number of occurrences of AE parameters recorded during the experiments), the range between 40 and 50 dB of amplitude was the one characterised by the highest number of events for all the samples. The counts parameter had a more variable tendency, with two ranges characterised by a greater number of events, the first with 10<=C<20 and the latter with C>30.

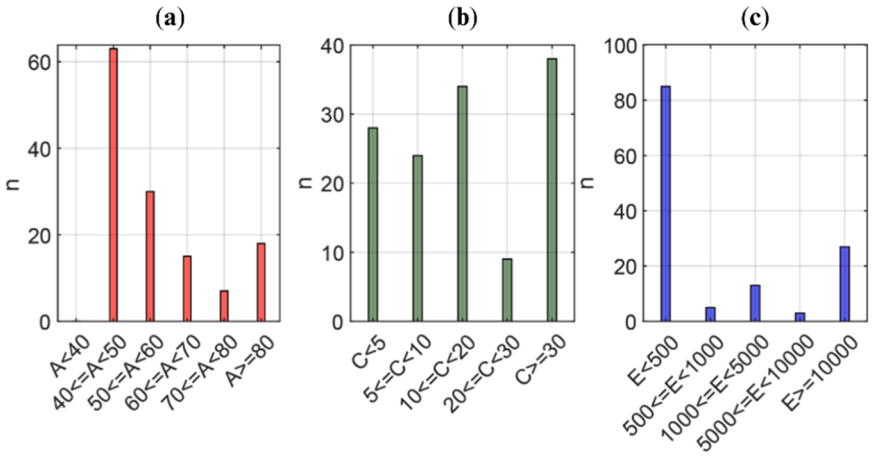

Fig. 6. Number of occurrences of AE parameters (time domain) during the experiment on sample H20PA4. (**a**) Amplitude (A), (**b**) Counts (C) and (**c**) Energy (E).

The distribution of the energy showed a peak for the class with E<500 (e.u.) confirmed by all the detections on the different tested samples. In Fig. 6, the case of sample "H20PA4" is again reported as an example, while frequency distribution of the whole set of samples is reported in Figs. A1 and A2 in Appendix.

These data indicate that during the experiments, the period of low or zero AE activity, is greater in terms of number of events than the period of high activity (corresponding to crack initiation and propagation) limited to a narrow number of events concentrated within an approximately short time interval. Moreover, the number of occurrences for each class of values tends to increase for samples with higher GA (in both high- and low- TRN).

The behaviour of the 15 samples during the fracture process is shown in Fig. 7 where different colours are used to indicate samples with different grain angles in both upper and lower panels. Small numbers above each curve refer specifically to the number of tree rings for each different sample. Higher values of load (from UTM) were reached by samples with higher grain angles, both in high (Fig. 7, upper panel) and low (Fig. 7, lower panel) TRN groups. Specifically, it is worth noticing that the higher the TRN of the sample, the higher the load values reached (from UTM), except for one of the L60PA samples (high load value with very low TRN).

In addition, it was observed that as the crack had time to propagate, the load progressively decreased (as in the case of 0°-20° and some of the 40° samples); on the contrary, when the fracture of samples was instantaneous, the propagation did not occur and so the load did not decrease (as in the case of 60° samples). In this latter case, the last load value was the maximum one recorded at the crack initiation point. Then, higher values of load and time were needed to trigger crack initiation in samples with higher grain angles and with higher tree rings (i.e., the case of 60° grain angle samples). Moreover, lowest values of TRN (4 for low TRN and 12 for high TRN) are characterised by earlier crack initiation and progressively decreasing load (as the crack progressively propagates). On the contrary, highest values of TRN (9 for low TRN and 24 for high TRN) are mostly characterised by instantaneous occurrence of fracture in the sample (no decreasing trend in the load parameter). The TRN parameter appeared to be not as influent as the GA one: in fact, at almost equal TRN, the samples' fracture behaviour depends on GA. Indeed, when TRN ranges between 9 and 12 or even within the same TRN group, the fracture behaviour is instantaneous at GA = 60° and progressive at GA ≤ 40°. This means that TRN is not a discriminating parameter of the fracture behaviour.

The same patterns occurred for the Density Linear energy Value (DLV) reported in Fig. 8. Its peak was reached for all the samples, at the crack initiation point (high emission of energy by a very small linear fracture) and then progressively decreased as the crack propagates. For samples with high GAs and high TRN (Fig. 7, upper panel), the DLV

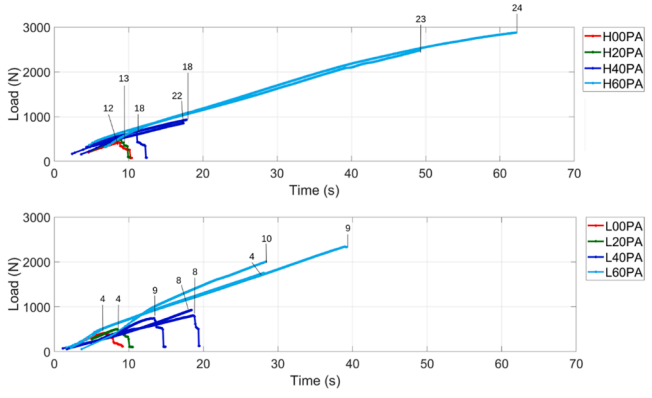

Fig. 7. Load *vs* time for (upper panel) high - and (lower panel) low - tree rings number samples. The small numbers above each curve refer specifically to the number of tree rings for each different sample.

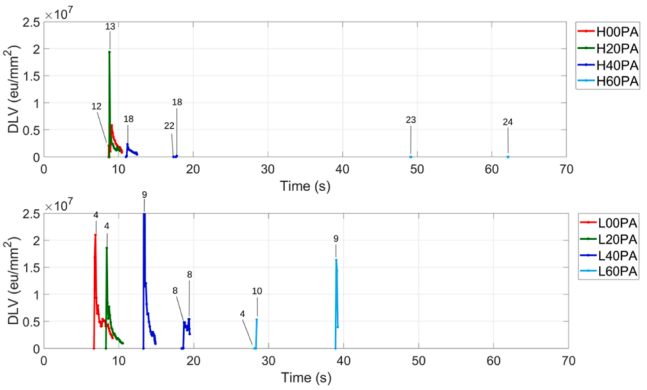

Fig. 8. Density Linear energy Value *vs* time for (top plot) high - and (bottom plot) low - tree rings number samples. The small numbers above each curve refer specifically to the number of tree rings for each different sample.

rapidly varied from zero to a small value (the crack emitted little energy). Again, the DLV parameter reached highest peaks in samples characterised by the lowest values of TRN (for both high and low TRN groups even if this is especially true for the first one). Fig. 8 also support the assessment of a major influence exerted by the GA parameter over the TRN one.

3.2. Identification of the early warning (EW) detection method

3.2.1. Early warning process characterisation

In Figs. 9a-b, the two different time intervals of the fracture process of each sample (i.e., time elapsed between the start of the experiment and the fracture initiation at macro-level (Δt_1) and time elapsed between the crack initiation point and the instant of the complete fracture (Δt_2)) are shown according to the different tree rings number (also shown by * for low TRN group and △ for high TRN group), also differentiated according to different grain angle categories (different color code).

In Fig. 9a, for both high and low TRN groups, $\Delta t_1 < 10$s for samples with GA < 40°, 10s < Δt_1 < 20s for GA = 40° and $\Delta t_1 > 20$s for GA = 60°. The fracture in Mode I occurs faster than in mixed Mode. No differences in terms of Δt_1 exist for different TRN values of the same GA category (in the cases of 0°, 20° and 40°), again indicating that the most influencing factor is GA of the samples. It is worth noting that for GA = 60° (light blue indicators), a longer Δt_1 is occurring in high TRN group ($\Delta t_1 > 45$s) rather than in low (25s < Δt_1 < 45s).

In Fig. 9b, Δt_2 was close to zero with the lowest variability for GA = 60° (mixed Mode) in all TRN groups, while $\Delta t_2 > 1$s for GA ≤ 20s. It is worth noticing that when GA = 40° Δt_2 ranges between 0 and 2s representing an intermediate condition. Once again, TRN parameter cannot be used as discriminant of the fracture behaviour.

3.2.2. Identification of an a posteriori EW threshold

The evolution of fracture process through the second derivative (f') of AE cumulative parameters (A, E, C) was investigated to discriminate abrupt changes in AE during the first-time interval (Δt_1). Fig. 10 shows f' (light blue lines) of two samples with high TRN: (a) "H00PA5" for fracture Mode I and (b) "H60PA6" for mixed Mode. In both samples, abrupt changes (blue lines) started occurring after 7s. However, a lower number of such events was recorded in fracture Mode I with respect to mixed Mode, which had higher occurrences and more lasting AE activity before the crack initiation (black dashed vertical line).

The number of occurrences of AE parameters (A, E and C) signals higher than 68th percentile is shown in Fig. 11 for samples "H00PA5" and "H60PA6" where an intensification of AE parameters (green bins) before the crack initiation point (dashed line) is visible for both samples. The increasing number of events shows the progressive acoustic activity

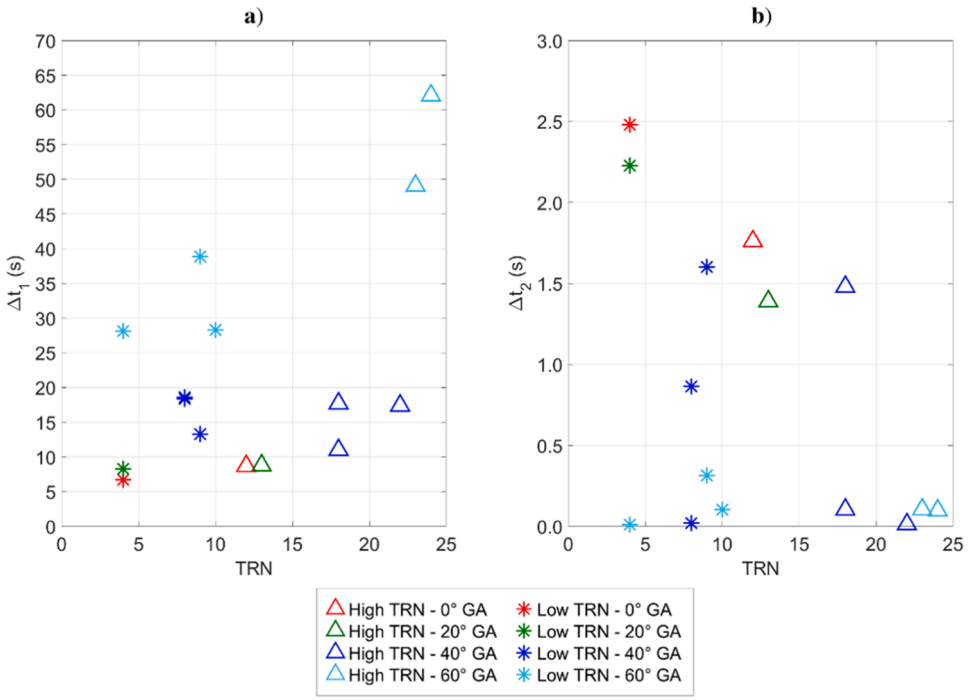

Fig. 9. (**a**) First and (**b**) second time intervals of the fracture process *vs* tree rings number.

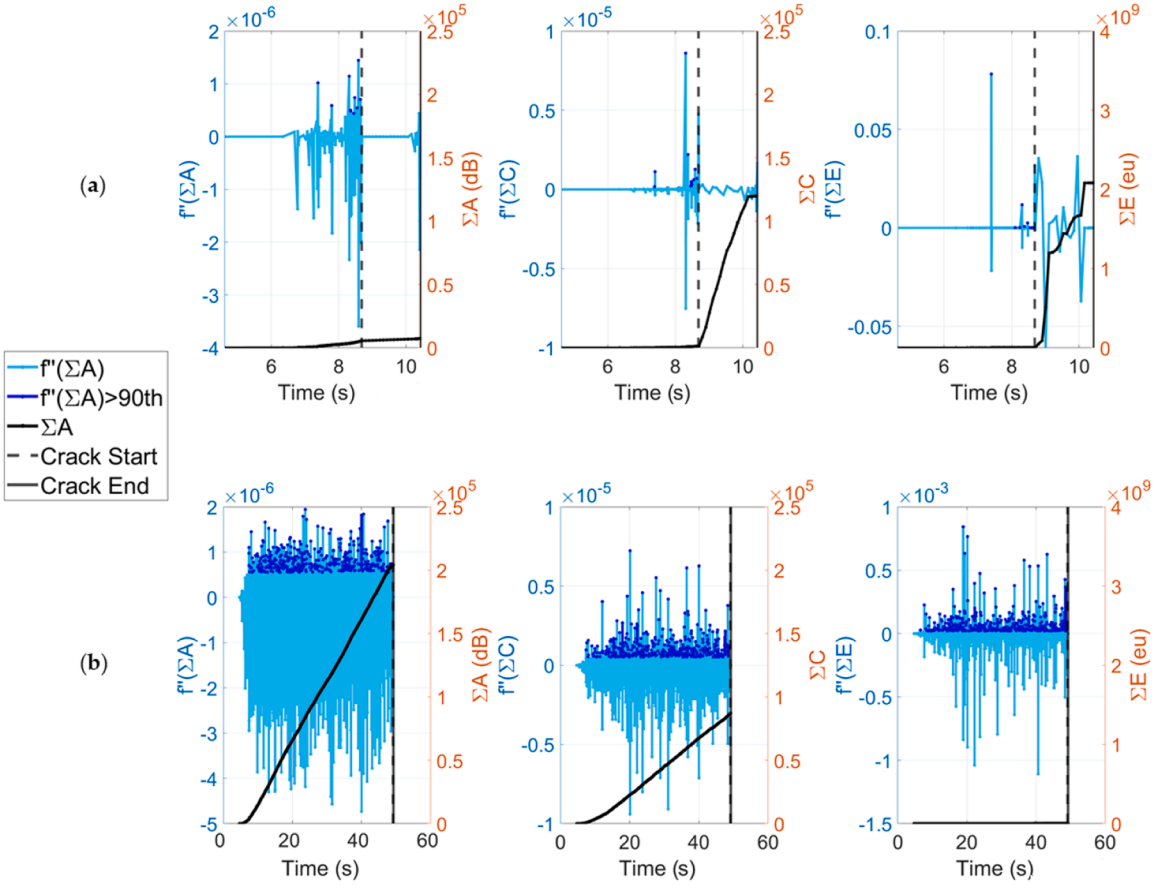

Fig. 10. Second derivative (f'') of AE cumulative parameters (i.e., ΣA-ΣC-ΣE) *vs* time for (**a**) "H00PA5" and for (**b**) "H60PA6".

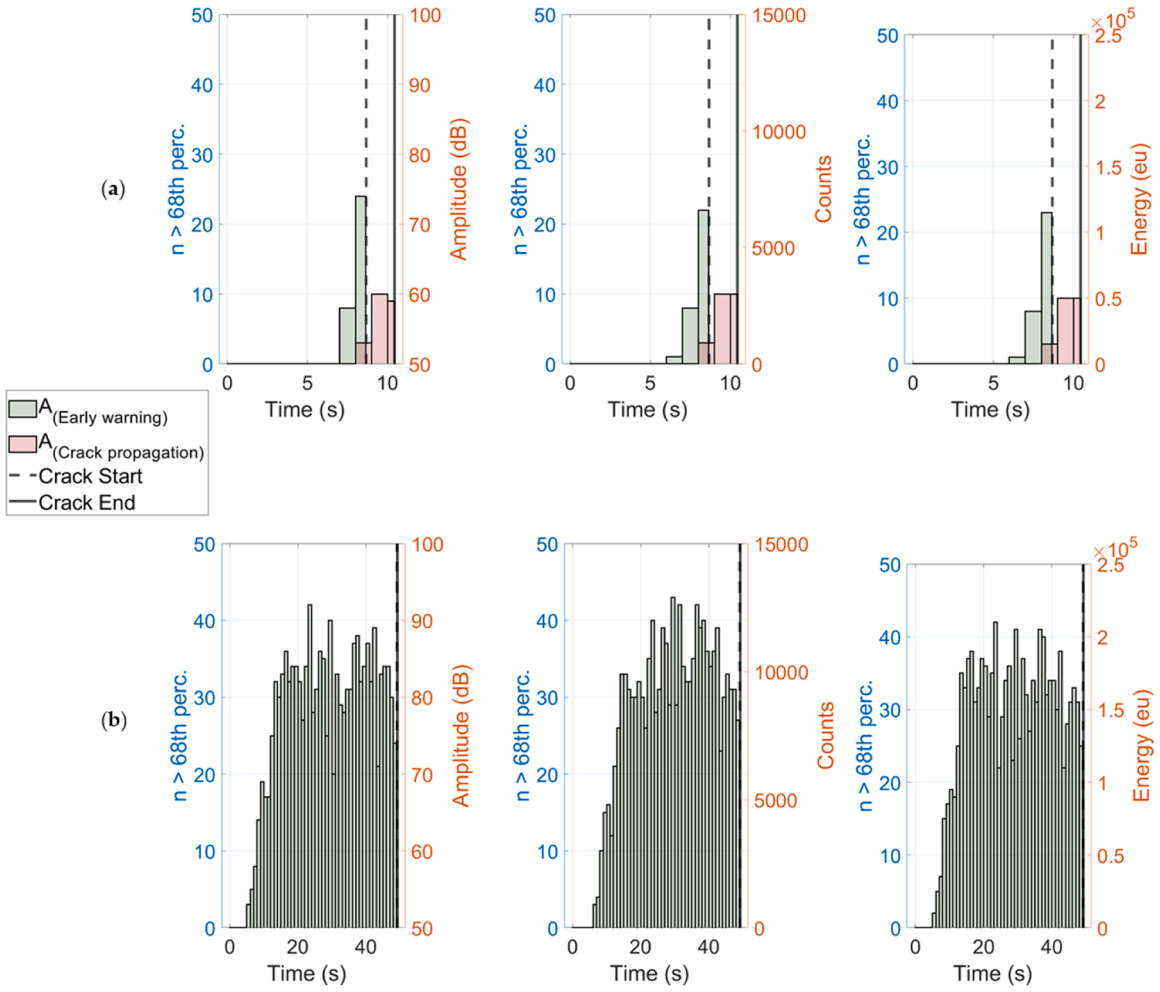

Fig. 11. Number of occurrences of AE parameters >68th percentile *vs* time for (**a**) "H00PA5" and for (**b**) "H60PA6".

during the EW stage, providing the warning on the imminence of the fracture that would soon occur. Although only for low GA samples (for which there was detectable crack propagation), the increasing activity also occurred during the crack propagation period up to the complete fracture as it is indicated by the pink bins in Fig. 11a, between the vertical dashed line (representative of the fracture initiation at macroscopic level) and the vertical solid line (representative of the completion of the fracture - broken sample). On the contrary, no increasing acoustic activity is recorded for high GA samples between the beginning of the propagation and the completion of the fracture, as these samples fracture abruptly (no pink bins between the two – dashed and solid – lines in Fig. 11b).

Finally, from the comparison between the histograms, it was also clear how as the GA increased (for both the TRN groups), the EW acoustic activity prior to the crack initiation tended to anticipate much more over time, with a higher number of events per second, thus enhancing the early warning capacity of the AE technique, which becomes maximum in case of mixed Mode fracture.

It may be noted that in some cases histogram bins graphically appear as cut, as the number of occurrences greater than the 68th percentile was calculated on the total number of events occurring second by second. Where the bins appear to be cut, it is because the count of the events on the time interval of a second was interrupted by the occurrence of the fracture.

The amplitude (A) can be considered the most sensitive AE parameter recorded during these experiments. The 68th percentile value of amplitude (A_{68th}), before the crack initiation, was extracted for all the 15 tested samples, representing the threshold beyond which AE activity began to increase in view of the forthcoming initiation. This method can be applied only when the fracture initiation occurs, so it cannot be used as an indicator to define an EW time interval *a priori*.

For this reason, the median value of A_{68th} was computed and used as threshold to define the start of the time interval expected before the fracture initiation in Scots pine SENT samples. The resulting threshold was A = 51.9 dB meaning that, when such value is recorded, a macrocrack can be expected in a certain time interval corresponding to the so-called early warning time (Δt_{ew}).

Δt_{ew} (Eq. (3)) is therefore defined as the EW time elapsed between

Table 2
Early warning (EW) time intervals for each of the 15 samples. The first column shows the grain angle value; the second column indicates the high TRN group for which the names of the samples with respective time intervals are reported below; in the third column the same is presented for low TRN samples. Numbers between brackets indicate the specific tree rings number of each sample.

Grain angle (°)	High tree rings number (TRN)		Low tree rings number (TRN)	
	Samples	*ΔT_{ew} (s)*	*Samples*	*ΔT_{ew} (s)*
0	H00PA5 (12)	1.6	L00PA5 (4)	3.1
20	H20PA4 (13)	2.5	L20PA4 (4)	2.7
	H40PA4 (18)	3.5	L40PA4 (9)	5.9
40	H40PA7 (18)	10.8	L40PA5 (8)	10.4
	H40PA6 (22)	12.9	L40PA6 (8)	15.7
	H60PA6 (24)	43.4	L60PA4 (10)	17.4
60	H60PA5 (23)	53.6	L60PA5 (4)	22.8
			L60PA6 (9)	33.3

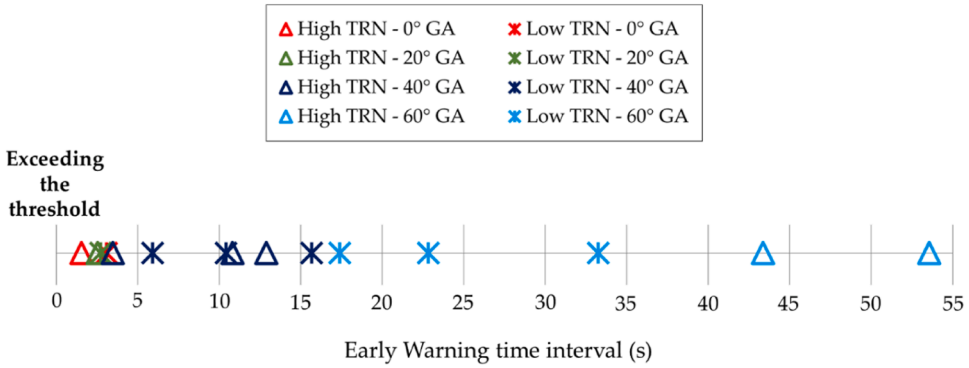

Fig. 12. Summary diagram of the early warning (EW) time intervals of each sample.

the crossing instant of the established threshold (51.9 dB) and the instant of the crack initiation. Δt_{ew} values were calculated for each of the 15 samples and reported in Table 2 and Fig. 12. Fig. 12 specifically reports a summary diagram of the early warning (EW) time intervals of each sample. Samples are here differentiated according to TRN by means of two different markers (* for low TRN and △ for high TRN) and according to GA values by four different colours (red for 0°, green for 20°, blue for 40°, sky blue for 60°).

The higher GA samples representative for mixed Mode fracture had the longest Δt_{ew} (>20s up to 54s) between the exceeding of the threshold and the crack initiation point. On the other extreme, GA = 0° samples, representative of Mode I fracture, admitted no possibility of predicting the oncoming fracture, due to the very short duration of Δt_{ew}. At the same time, the high TRN seems to have an influence above all on the 60° grain angle samples, for which it caused a greater resistance and led to the longest early warning time interval among the tested samples.

4. Conclusions

The preliminary analysis of combined Acoustic Emission technique, Digital Image Correlation camera and Universal Testing Machine data yielded the following information:

- Higher values of time and load are required to produce crack initiation in samples with high grain angles (i.e., mixed Mode), and with high tree rings number. At the same time, load and Density Linear energy Value (DLV) factors reach their peaks at the crack initiation points when the load is maximum and a large emission of energy by a small crack propagation happens suddenly (i.e., maximum in second derivative - in the acceleration of the emission).
- Once external load is applied, grain angle (GA) = 0° (Mode I fracture) fractures itself earlier than higher grain angle samples (mixed Mode fracture) allowing a lower possibility of predicting the oncoming fracture. However, there is a propagation before the complete fracture in the first case, while in the second case the complete fracture occurs suddenly.
- Only for samples with GA = 60° a higher tree rings number (TRN) also means major resistance to fracture (longest time interval prior to crack initiation). In the meanwhile, no significant differences were found for samples belonging to all the other GA categories (0-20-40°) at different tree rings number, meaning that the most influencing factor in the fracture behaviour of samples is GA.
- The median value of 68^{th} percentiles of the amplitude (A) of all samples was defined as a risk threshold computed here experimentally *a posteriori*, by causing the fracture of tested materials. The resulting value (A = 51.9dB) can be taken as a reference and applied to predict the occurrence of fracture in the same material or very similar ones (with comparable features of grain angle values and tree rings number), which respond equally to the stresses caused by the application of a force (thus becoming in this case, an *a priori* risk threshold).

From this evaluation, a threshold is discriminated to be used as an early warning indicator able to potentially predict at which time after it is exceeded the crack occurs in the samples, according to their different tree rings number and grain angles. This method, which is more immediate because it focuses on the pure signal of the parameters, nevertheless has the limitation of being able to be applied only after the experiment is completed, meaning that the sample has already broken Moreover, the random speckle pattern applied to the samples in order to employ DIC system did not allow a clear discrimination of microcracks related to the development of a fracture process zone (FPZ).

It can however be said that when choosing a material to be used for a conservative application or even as a building construction material, it would be more appropriate to direct the choice towards a wood material with high grain angle and high tree rings number, which is more resistant to fracture and allows greater possibility of early detection. At the same time, the drawback aspect of such choice should be considered for this same type of material: once the crack initiation point is reached, the crack propagates very quickly (so that it can be considered instantaneous as in the case of the tested samples). This underlines how important it is to avoid this kind of situation, adopting NDT techniques as far as possible as preventive monitoring tools to detect the status of stress impact on wooden materials.

In conclusion, AE NDT technique is proved to be useful as an early warning (EW) method in predicting fractures before their occurrence. Future research could eventually improve the accuracy of the EW threshold here proposed, by considering a higher number of specimens or by conducting validation with an identical set of samples. Similarly, upcoming research investigations could be performed in different real conditions to gain insights on how the early warning capability of AE technique varies depending on the variables considered.

Funding

This research was funded by the Norwegian Research Council within the Symbol project, grant number 274749 and by the European Union's Horizon 2020 research and innovation programme within the CollectionCare project, grant number 814624.

CRediT authorship contribution statement

Giulia Boccacci: Methodology, Formal analysis, Data curation, Writing – original draft. **Francesca Frasca:** Methodology, Writing – review & editing. **Pasi Aalto:** Resources. **Chiara Bertolin:** Resources, Writing – review & editing, Funding acquisition. **Anna Maria Siani:** Methodology, Writing – review & editing.

Declaration of Competing Interest

The authors declare that they have no known competing financial interests or personal relationships that could have appeared to influence the work reported in this paper.

Data availability

Data will be made available on request.

Acknowledgements

C.B. is indebted to the technical staff of the NTNU Wood Centre. Special thanks to Dr. P. Karvan, who while employer at NTNU within the SyMBoL project, helped in collecting data from tensile tests conceived by the principal researcher and coordinator of the SyMBoL Project. C.B. acknowledges the support of the Norwegian Research Council through the SyMBoL Project (project no. 274749). F.F. acknowledges fellowship funding from MUR (Ministero dell'Università e della Ricerca) under PON "Ricerca e Innovazione" 2014-2020 (D.M. 1062/2021). G.B. is indebted to the Erasmus+ Traineeship exchange program. A.M.S. has received funding from the European Union's Horizon 2020 research and innovation programme under grant agreement N. 814624.

Appendix

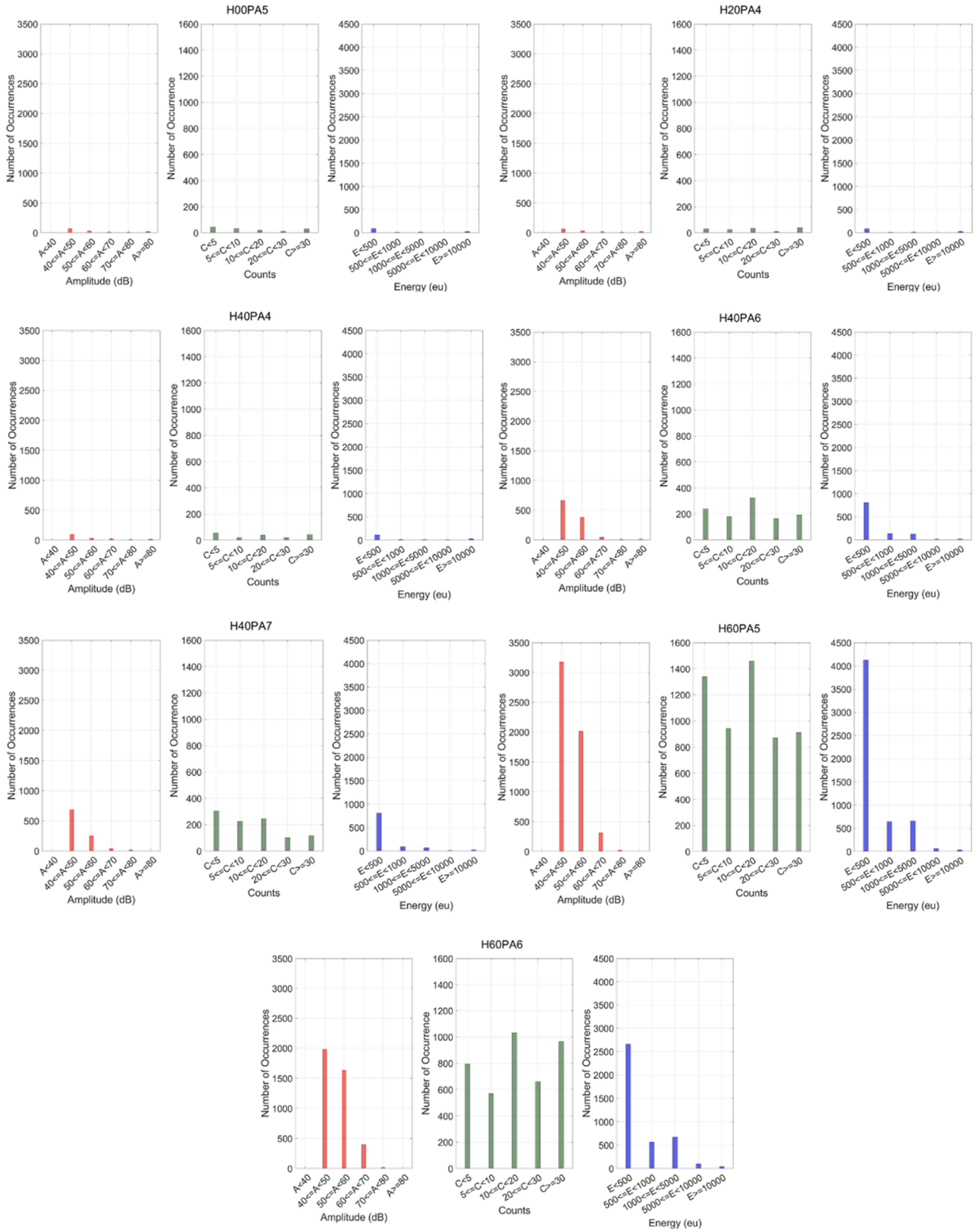

Fig. A1. Number of Occurrences for AE parameters of Amplitude (A), Counts (C) and Energy (E) – High number of tree rings samples.

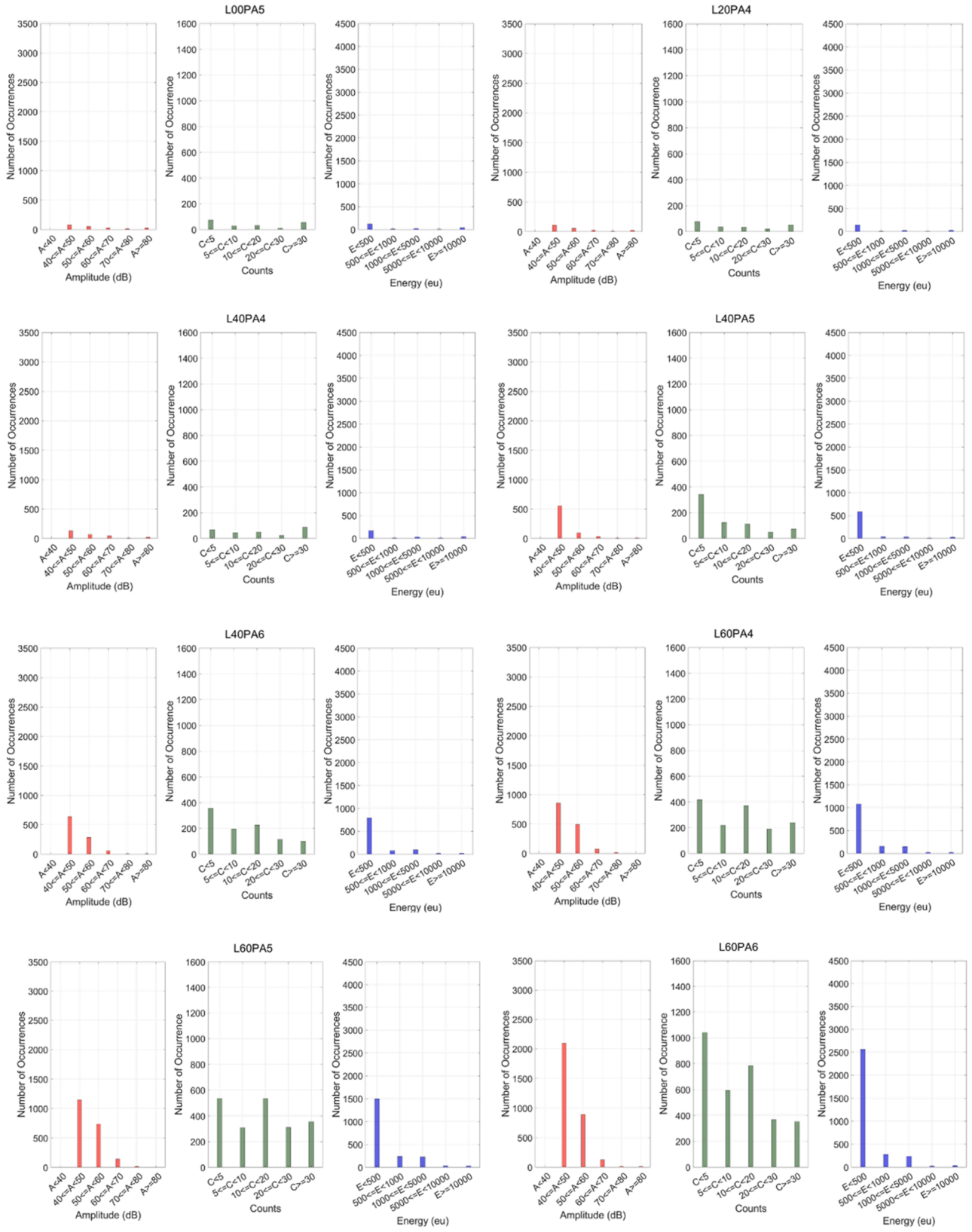

Fig. A2. Number of Occurrences for AE parameters of Amplitude (A), Counts (C) and Energy (E) – Low number of tree rings samples.

References

[1] G. Boccacci, F. Frasca, C. Bertolin, A.M. Siani, Influencing factors in acoustic emission detection: a literature review focusing on grain angle and high/low tree ring density of scots pine, Appl. Sci. 12 (2022) 859, https://doi.org/10.3390/app12020859.

[2] P Kossakowski, Fracture toughness of pine wood for I and II loading modes, Arch. Civil Eng. 54 (2008) 509–529.

[3] M.P.C. Conrad, Fracture of solid wood: a review of structure and properties at different length scales, Wood Fiber Sci. 35 (2003) 570–584.

[4] N. Dourado, S. Morel, M.F.S.F. de Moura, G. Valentin, J. Morais, Comparison of fracture properties of two wood species through cohesive crack simulations, Compos. Part A Appl. Sci. Manuf. 39 (2008) 415–427, https://doi.org/10.1016/j.compositesa.2007.08.025.

[5] M.F.S.F. de Moura, J.J.L. Morais, N. Dourado, A new data reduction scheme for mode i wood fracture characterization using the double cantilever beam test, Eng. Fract. Mech. 75 (2008) 3852–3865, https://doi.org/10.1016/j.engfracmech.2008.02.006.

[6] M.F.S.F. de Moura, N. Dourado, Mode I fracture characterization of wood using the TDCB test, Theor. Appl. Fract. Mech. 94 (2018) 40–45, https://doi.org/10.1016/j.tafmec.2018.01.005.

[7] H. Yoshihara, Mode II R-curve of wood measured by 4-ENF test, Eng. Fract. Mech. 71 (2004) 2065–2077, https://doi.org/10.1016/j.engfracmech.2003.09.001.

[8] H. Yoshihara, Theoretical analysis of 4-ENF tests for Mode II fracturing in wood by finite element method, Eng. Fract. Mech. 75 (2008) 290–296, https://doi.org/10.1016/j.engfracmech.2007.03.043.

[9] Stanzi-Tschegg, S.E.; Tan, D.M.; Tschegg, E.K. *New splitting method for wood fracture characterization*; 1995; Vol. 29;.

[10] E. Stefanie, D.-M.T.E.K.T. Stanzl-Tschegg, Fracture Resistance to the Crack Propagation in Wood, 75, Kluwer Academic Publ&hers, 1996.

[11] M. Fakoor, N.M. Khansari, A new approach for investigation of Mode II fracture toughness in orthotropic materials, Latin Am. J. Solid. Struct. (2018) 15, https://doi.org/10.1590/1679-78253979.

[12] M. Fakoor, S. Shahsavar, Fracture assessment of cracked composite materials: progress in models and criteria, Theor. Appl. Fract. Mech. (2020) 105, https://doi.org/10.1016/j.tafmec.2019.102430.

[13] Baensch F. Damage Evolution in Wood and Layered Wood Composites Monitored in Situ by Acoustic Emission, Digital Image Correlation and Synchrotron Based Tomographic Microscopy. PhD Thesis, ETH Zürich, Zürich, Switzerland, 2015.

[14] M. Lukomski, M. Strojecki, B. Pretzel, N. Blades, V.L. Beltran, A. Freeman, Acoustic emission monitoring of micro-damage in wooden art objects to assess climate management strategies, Insight: Non-Destruct. Test. Condit. Monitor. 59 (2017) 256–264, https://doi.org/10.1784/insi.2017.59.5.256.

[15] M. Perrin, I. Yahyaoui, X. Gong, Acoustic monitoring of timber structures: influence of wood species under bending loading, Constr. Build. Mater. 208 (2019) 125–134, https://doi.org/10.1016/j.conbuildmat.2019.02.175.

[16] A. Reiterer, G. Sinn, S.E. Stanzl-Tschegg, Fracture characteristics of different wood species under Mode I loading perpendicular to the grain, Mater. Sci. Eng. 332 (2002) 29–36, https://doi.org/10.1016/s0921-5093(01)01721-x.

[17] C. Bertolin, L. de Ferri, J. Razavi, F. Berto, Acoustic emission NDT for monitoring hygro-mechanical reactions of coated pine wood: a methodological approach, in: Proceedings of the Procedia Structural Integrity 28, Elsevier B.V., 2020, pp. 208–217. Vol.

[18] S. Jan Kowalski, A Smoczkiewicz, Acoustic emission in wood under drying, Seria B, Zeszyt 35 (2004) 59–71.

[19] S. Rosner, Waveform features of acoustic emission provide information about reversible and irreversible processes during spruce sapwood drying, Bioresources 7 (2012) 1253–1263, https://doi.org/10.15376/BIORES.7.1.1253-1263.

[20] R.W. Rice, D.P. Phillips, Estimating the moisture excluding effectiveness of surface coatings on southern yellow pine using acoustic emission technology, Wood Sci. Technol. 34 (2001) 533–542, https://doi.org/10.1007/s002260000057.

[21] W. Moliński, J. Raczkowski, L. Muszyński, Acoustic emission generated upon mechano-sorptive creep of wood bent across to the grain under asymmetrical moistening, Holzforschung 34 (2000) 305–308, https://doi.org/10.1515/hf.2000.051.

[22] F.J. Rescalvo, L. Morillas, I. Valverde-Palacios, A. Gallego, Acoustic emission in I-214 poplar wood under compressive loading, Eur. J. Wood Wood Prod. 78 (2020) 723–732, https://doi.org/10.1007/s00107-020-01536-7.

[23] Z. Shao, F. Wang, Fractal features and acoustic emission characteristics of wood fracture. The Fracture Mechanics of Plant Materials, Springer, Singapore, 2018, pp. 103–124.

[24] K. Ando, Y. Hirashima, M. Sugihara, S. Hirao, Y. Sasaki, Microscopic processes of shearing fracture of old wood, examined using the acoustic emission technique, J. Wood Sci. 52 (2006) 483–489, https://doi.org/10.1007/s10086-005-0795-7.

[25] A. Kánnár, The effect of moisture content on the micro-damage processes of spruce wood, investigated by acoustic emission method and electron microscopy, Acta Silv. Lign. Hung. 2 (2006) 93–104.

[26] P. Karvan, S.M.J. Razavi, F. Berto, C. Bertolin, Energy density and fracture parameters of coated scots pine, Constr. Build. Mater. (2021) 290, https://doi.org/10.1016/j.conbuildmat.2021.123206.

[27] F.J. Rescalvo, M. Rodríguez, R. Bravo, C. Abarkane, A. Gallego, Acoustic emission and numerical analysis of pine beams retrofitted with FRP and poplar wood, Materials (2020) 13, https://doi.org/10.3390/ma13020435.

[28] P.G. Kossakowski, Mixed Mode I/II fracture toughness of pine wood, Arch. Civil Eng. 55 (2009) 199–227.

[29] A. Aguilera, M. Vega, P.J. Méausoone, Effects of grain angle on the amplitudes of acoustic emission and surface roughness in wood machining, Wood Sci. Technol. 41 (2007) 373–381, https://doi.org/10.1007/s00226-006-0117-2.

[30] C. Bertolin, L. de Ferri, F. Berto, Calibration method for monitoring hygro-mechanical reactions of pine and oak wood by acoustic emission nondestructive testing, Materials (2020) 13, https://doi.org/10.3390/MA13173775.

[31] S. Aicher, L.H. Ĕfflin, G. Dill-Langer, Damage evolution and acoustic emission of wood at tension perpendicular to fiber, Eur. J. Wood Wood Prod. 59 (2001) 104–116, https://doi.org/10.1007/s001070050482.

[32] A. Marec, J.H. Thomas, R. El Guerjouma, Damage characterization of polymer-based composite materials: multivariable analysis and wavelet transform for clustering acoustic emission data, Mech. Syst. Signal Process. 22 (2008) 1441–1464, https://doi.org/10.1016/j.ymssp.2007.11.029.

[33] M. Wang, M. He, Z. Liang, D. Wu, Y. Wang, X. Qing, Y. Wang, Fatigue damage monitoring of composite laminates based on acoustic emission and digital image correlation techniques, Compos. Struct. (2023) 321, https://doi.org/10.1016/j.compstruct.2023.117239.

[34] S. Ashraf, S. Khan, V.K. Oad, Microcracking monitoring and damage detection of graphene nanoplatelets-cement composites based on acoustic emission technology, Case Stud. Construct. Mater. 18 (2023), https://doi.org/10.1016/j.cscm.2023.e01844.

[35] Z. Chen, B. Gabbitas, D. Hunt, Monitoring the fracture of wood in torsion using acoustic emission, J. Mater. Sci. 41 (2006) 3645–3655, https://doi.org/10.1007/s10853-006-6292-6.

[36] B. Bartolucci, A. de Rosa, C. Bertolin, F. Berto, F. Penta, A.M. Siani, Mechanical properties of the most common European woods: a literature review, Frattura ed Integrita Strutturale 14 (2020) 249–274.

[37] MTS Criterion® series 40 electromechanical universal test systems. Available Online: https://Test.Mts.Com/-/Media/Materials/Pdfs/Brochures/100-262-929d_criterionem40.Pdf?As=1 (Accessed on 15 May 2021).

[38] Stingray. The transformer camera. Available Online: https://www.1stvision.Com/Cameras/AVT/Dataman/Stingray_DataSheet_F504BC_fiber_V1.1.1.Pdf (Accessed on 15 May 2021).

[39] AMSY-6 system description. Available Online: https://www.Vallen.de/Zdownload/Pdf/AMSY-6_Description.Pdf (Accessed on 15 May 2021).

[40] F. Frasca, A.M. Siani, G.R. Casale, M. Pedone, Bratasz, M. Strojecki, A Mleczkowska, Assessment of indoor climate of Mogiła abbey in Kraków (Poland) and the Application of the analogues method to predict microclimate indoor conditions, Environ. Sci. Pollut. Res. 24 (2017) 13895–13907, https://doi.org/10.1007/s11356-016-6504-9.

[41] Q. Zhao, D. Zhao, J. Zhao, Thermodynamic approach for the identification of instability in the wood using acoustic emission technology, Forests (2020) 11, https://doi.org/10.3390/F11050534.

[42] L.F. Friedrich, B.N.R. Tanzi, A.B. Colpo, M. Sobczyk, G. Lacidogna, G. Niccolini, I. Iturrioz, Analysis of acoustic emission activity during progressive failure in heterogeneous materials: experimental and numerical investigation, Appl. Sci. (Switzerland) (2022) 12, https://doi.org/10.3390/app12083918.

[43] S.K. Kourkoulis, I. Dakanali, Pre-failure indicators detected by acoustic emission: alfas stone, cement-mortar and cement-paste specimens under 3-point bending, Frattura ed Integrita Strutturale 11 (2017) 74–84, https://doi.org/10.3221/IGF-ESIS.40.07.

[44] V.L. Shkuratnik, P.V. Nikolenko, A.E. Koshelev, Spectral characteristics of acoustic emission in loaded coal specimens for failure prediction, J. Min. Sci. 53 (2017) 818–823, https://doi.org/10.1134/S1062739117052825.